

BISTABLE OSCILLATIONS ARISING FROM SYNAPTIC DEPRESSION*

AMITABHA BOSE[†], YAIR MANOR[‡], AND FARZAN NADIM[§]

Abstract. Synaptic depression is a common form of short-term plasticity in the central and peripheral nervous systems. We show that in a network of two reciprocally connected neurons a single depressing synapse can produce two distinct oscillatory regimes. These distinct periodic behaviors can be studied by varying the maximal conductance, \bar{g}_{inh} , of the depressing synapse. For small \bar{g}_{inh} , the network has a short-period solution controlled by intrinsic cellular properties. For large \bar{g}_{inh} , the solution has a much longer period and is controlled by properties of the synapse. We show that in an intermediate range of \bar{g}_{inh} values both stable periodic solutions exist simultaneously. Thus the network can switch oscillatory modes either by changing \bar{g}_{inh} or, for fixed \bar{g}_{inh} , by changing initial conditions.

Key words. synaptic plasticity, inhibition, excitation, neuromodulation, bistability

AMS subject classifications. 92C20, 34C15, 34C26

PII. S0036139900378050

1. Introduction. Although synapses are commonly modeled to be linear transfer functions between two neurons, it is now widely recognized that synapses are nonlinear dynamic devices. Chemical synapses express various forms of short-term dynamics such as use-dependent facilitation and depression (reviewed in [39]). Use-dependent synaptic depression is ubiquitous in all nervous systems. This form of synaptic plasticity is usually defined as a reduction in the amplitude of the synaptic conductance in response to the firing of action potentials (spikes) in the presynaptic neuron: the synaptic current in response to each spike within a burst is smaller than the previous one. Although the mechanisms underlying synaptic depression have been studied extensively, its functional significance is mostly unknown. Several computational and theoretical studies have proposed that synaptic depression can be used in various tasks, such as dynamic gain control [1, 34], burst detection [21], sequence determination [7], and rhythmogenesis [32].

The dynamics of synaptic depression were recently characterized in an experimental study of the rhythmically active pyloric network of the spiny lobster [22]. This study showed that, because of depression, synaptic efficacy in a rhythmic network depends nonlinearly on the frequency of the network and the duty cycles of the neurons involved. Using these results, Nadim et al. [27] demonstrated that synaptic depression can be used as a switch mechanism between two modes of oscillation

*Received by the editors September 13, 2000; accepted for publication (in revised form) April 10, 2001; published electronically December 4, 2001.

<http://www.siam.org/journals/siap/62-2/37805.html>

[†]Department of Mathematical Sciences, Center for Applied Mathematics and Statistics, New Jersey Institute of Technology, Newark, NJ 07102 (bose@m.njit.edu). The research of this author was supported in part by NSF grant DMS-9973230 and NJIT grant 421540.

[‡]Life Sciences Department, Ben-Gurion University of the Negev and Zlotowski Center for Neuroscience, Beer-Sheva, Israel 84105 (yairman@bgumail.bgu.ac.il). The research of this author was supported in part by the Israel Science Foundation grant 314/99-1 and the Zlotowski Center for Neuroscience.

[§]Department of Mathematical Sciences, Center for Applied Mathematics and Statistics, New Jersey Institute of Technology, Newark, NJ 07102 and Department of Biological Sciences, Rutgers University, Newark, NJ 07102 (farzan@njit.edu). The research of this author was supported in part by the Alfred P. Sloan Foundation and NJIT grant 421140.

in reciprocally inhibitory rhythmic networks: a high-frequency oscillation controlled by intrinsic neuronal properties (cell-dominated) and a low-frequency oscillation controlled by the dynamics of depression (synapse-dominated).

Nadim et al. [27] provide a heuristic explanation for the mechanism that enables or disables the depressing synapse to control the network oscillations and produce bistability. There are, however, several questions that remain unanswered, the most important of which are as follows: What switches the network from one mode to the other? What parameters are important in each of the two modes? What mechanism gives rise to the bistability of periodic orbits? What values of parameters support bistability? Is the switch mechanism specific to inhibitory-inhibitory circuits, or can it be extended to other circuits as well? In this manuscript, we address these questions directly by using analytical tools.

Excitatory-inhibitory (EI) pairs of neurons are common elementary circuits in the mammalian brain. Such circuits are found in the sensory-motor cortex [16], the visual cortex [2], the hippocampus [3], the olivo-cerebellar system [36], the nucleus reticularis thalami [30], and so on. Often these circuits show rhythmic activity generated by intrinsic properties or emerging from network interactions. Due to the ubiquity of EI circuits, it is important to obtain a good understanding of the processes that control their output. This, together with the proposed role of synaptic depression in inhibitory-inhibitory loops [27], led us to address the existence of a switch mechanism and bistability of rhythmic activity in EI circuits that involve synaptic depression.

Our model consists of a reciprocally coupled pair of neurons: an oscillatory excitatory neuron E and a nonoscillatory inhibitory neuron I . We address the situation where the synapse from I to E is depressing and the synapse from E to I is strong and fast. We show that, depending on the maximal conductance, \bar{g}_{inh} , of the depressing synapse, two distinct oscillation modes emerge. When \bar{g}_{inh} is small, the depressing synapse remains weak, the rhythm is fast, and its frequency is controlled by the intrinsic properties of the E neuron. Alternatively, when \bar{g}_{inh} is large, the synapse is strong, the rhythm is slow, and its frequency is controlled by \bar{g}_{inh} and the time courses of the depressing synapse. Our analysis shows that the two modes coexist for an intermediate range of values of \bar{g}_{inh} if the intrinsic time constants of the neurons are much smaller than the decay and depression time courses of the synapse. Thus the network exhibits bistability of periodic orbits. The results of this work apply to more general EI networks, such as the case where the E to I synapse is depressing or when E is not an intrinsic oscillator.

The paper is organized as follows. In section 2, we describe the model of the depressing synapse and give the equations for the E and I cells. Here the geometric techniques that are used throughout the paper are described. In section 3, we prove that the EI network is bistable. We show that if the maximal conductance of the depressing synapse is too large or too small, then only a single stable solution persists. We also elaborate on how depression can be useful in other network architectures. In section 4, we compare our model of synaptic depression to previously proposed models. We then discuss implications of bistability and how the mechanism described in this work may be exploited by modulators of the activity of neuronal networks.

2. The model. The cells are modeled using standard biophysical current-balance equations. The rate of change of the membrane potential v is proportional to the sum of ionic currents flowing through the cell. Each ionic current is given as a product of a conductance and a driving force, the difference between v and a fixed equilibrium potential being associated with that current. Each cell in our model has a single non-

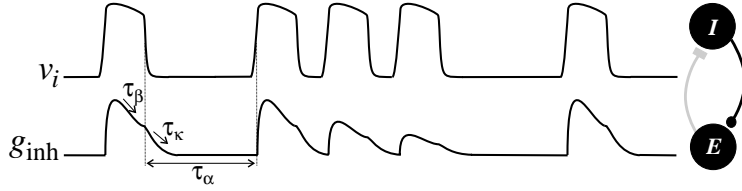


FIG. 1. Schematic diagram showing the definition and time courses of synaptic depression. Time traces of the membrane potential of the I cell and the synaptic conductance g_{inh} are shown. The time constants are, respectively, τ_β for depression, τ_α for recovery from depression, and τ_κ for the decay of the synapse when the I cell is not active.

linear intrinsic current in which the conductance is gated by the membrane potential of the cell. The “gating variable” w follows a simple differential equation given below. The biophysical equations and parameter values used for simulations are provided in the appendix. For the analysis below, we focus on the qualitative form of these equations. The qualitative behavior is extracted from the shape and position of the nullclines in the phase space of each cell.

The basic properties of our model of synaptic depression are shown schematically in Figure 1. Traces shown are the membrane potential v_i of the I neuron and the synaptic conductance of the depressing synapse (from I to E). When v_i crosses the threshold for synaptic release v_{thresh} , the conductance g_{inh} rapidly rises to a peak and then decays with a time course given by τ_β . The value of the peak is dependent not only on the maximum synaptic conductance \bar{g}_{inh} but also on the intrinsic and synaptic time constants. When v_i falls below the threshold for transmission, g_{inh} decays with time constant τ_κ . For the duration that v_i remains below the threshold, g_{inh} recovers from depression with time constant τ_α . The time constant τ_α is long compared to the intrinsic time constants of the I neuron. Therefore, if v_i is below the transmission threshold for a short duration, g_{inh} does not fully recover from depression, and the subsequent peak of g_{inh} will be smaller.

2.1. The neurons. Both the excitatory and the inhibitory neurons are modeled as two-dimensional singularly perturbed systems and have an active (high voltage) and a silent or inactive state. In dimensionless form, the neuron E is described using the equations

$$(2.1) \quad \begin{aligned} \epsilon v_e' &= f_e(v_e, w_e), \\ w_e' &= [w_\infty(v_e) - w_e]/\tau_e(v_e), \end{aligned}$$

where v_e denotes the voltage and w_e is the gating variable for the cell. The nonlinearity f_e consists of the sum of currents which are intrinsic to the cell. The parameter $\epsilon \ll 1$ is the singular perturbation parameter and the derivative is with respect to t . The v_e -nullcline, given by $\mathcal{C}_e = \{(v_e, w_e) : f_e(v_e, w_e) = 0\}$, is cubic shaped, whereas the w_e -nullcline, given by $\mathcal{S}_e = \{(v_e, w_e) : w_\infty(v_e) - w_e = 0\}$, is sigmoidal. We assume that these two curves intersect along the middle branch of the cubic \mathcal{C}_e , thus ensuring that an isolated E cell is oscillatory [29] (Figure 2). We denote the local minimum point, or left knee, of \mathcal{C}_e by (v_{LK}, w_{LK}) and the local maximum point, or right knee, of \mathcal{C}_e by (v_{RK}, w_{RK}) . The time constant τ_e is given by

$$(2.2) \quad \tau_e(v_e) = \begin{cases} \tau_R & \text{if } v_e > v_\theta, \\ \tau_L & \text{if } v_e < v_\theta, \end{cases}$$

where $v_\theta \in (v_{LK}, v_{RK})$ is the threshold for entering the active phase and τ_R and τ_L are the time constants during the active and silent phase, respectively. We assume

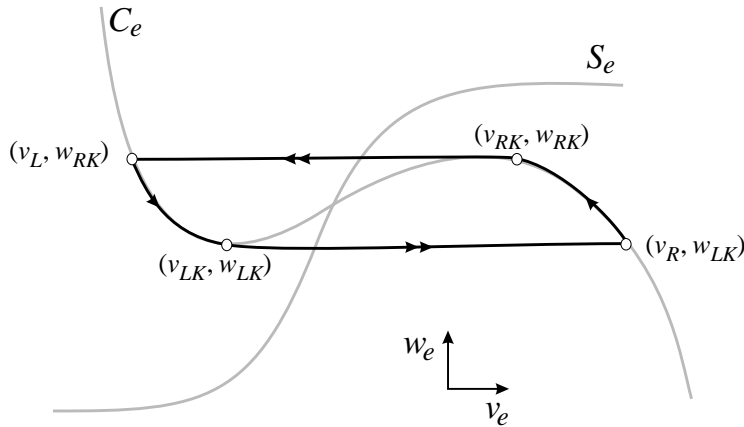


FIG. 2. Phase-plane diagram of the activity of the isolated E cell. C_e is the v_e -nullcline, and S_e is the w_e -nullcline. The solid trajectory is the singular periodic orbit consisting of slow movement of the solution along C_e and fast jumps from the left (v_{LK}, w_{LK}) and right (v_{RK}, w_{RK}) knees of C_e to the opposite branch.

that $f_e > 0$ (< 0) below (above) the cubic and $w_\infty(v_e) - w_e > 0$ (< 0) below (above) the sigmoid S_e .

We shall study the network dynamics in the phase space by exploiting the fact that the parameter ϵ is small, allowing us to use techniques of geometric singular perturbation theory. We first construct singular solutions by analyzing the reduced equations which are appropriately scaled versions of (2.1) when $\epsilon = 0$. Solutions of the reduced equations are pieced together to obtain a singular periodic orbit. Each piece of this orbit is a valid trajectory when $\epsilon = 0$. It is then necessary to show that for ϵ small and positive there is a periodic solution of (2.1) near the singular solution.

The reduced equations and singular periodic orbit for the isolated E cell are constructed as follows. The slow reduced equations are obtained by setting $\epsilon = 0$ in (2.1) to obtain

$$(2.3) \quad \begin{aligned} 0 &= f_e(v_e, w_e), \\ w'_e &= [w_\infty(v_e) - w_e]/\tau_e(v_e). \end{aligned}$$

These equations govern the evolution of E during its active or silent state. The first equation is algebraic and constrains E to lie on the cubic C_e . The second equation gives the direction and speed of the flow on the cubic.

The fast reduced equations are obtained by rescaling time in (2.1) by letting $\xi = t/\epsilon$ and then setting $\epsilon = 0$. This yields

$$(2.4) \quad \begin{aligned} \dot{v}_e &= f_e(v_e, w_e), \\ \dot{w}_e &= 0. \end{aligned}$$

Here the derivative is with respect to ξ . These equations govern the fast jumps between the active and silent states of the cell. Because of the second equation, w_e acts as a parameter in the first equation. Note that both the slow and the fast reduced equations are scalar differential equations. For the fast equations (2.4), the left and right branches of C_e are attracting, and the middle branch is repelling. The left knee is attracting from the left and repelling from the right; the opposite is true for the right knee.

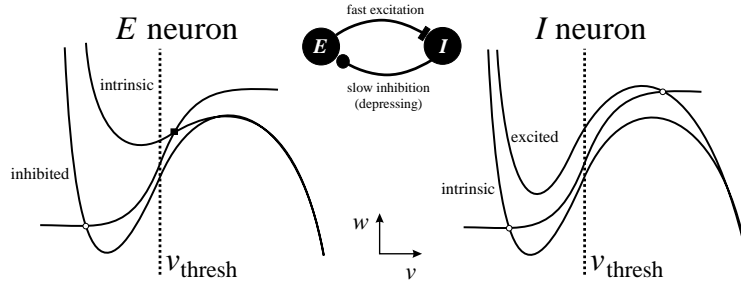


FIG. 3. The effect of synapses on the EI network. Each panel shows the v - and w -nullclines of the cells, both in isolation and in the presence of a fixed synaptic input. Inhibition of E lowers the cubic v -nullcline, whereas excitation of I raises this nullcline. v_{thresh} is the threshold for synaptic transmission. The stable and unstable fixed points are denoted by white circles and filled squares, respectively.

The singular periodic orbit for E can now be described as the union of the following four pieces (Figure 2). Starting at the left knee of \mathcal{C}_e , the first piece is a solution of (2.4) which connects (v_{LK}, w_{LK}) on the left branch of \mathcal{C}_e to (v_R, w_{LK}) on the right branch of \mathcal{C}_e . The second piece is a solution of (2.3) which connects (v_R, w_{LK}) to (v_{RK}, w_{RK}) on the right branch of \mathcal{C}_e . Notice that on the right branch of \mathcal{C}_e , $\dot{w}_e > 0$. The third piece is a solution of (2.4) which connects (v_{RK}, w_{RK}) on the right branch of \mathcal{C}_e to (v_L, w_{RK}) on the left branch of \mathcal{C}_e . The fourth and final piece is a solution of (2.3) which connects (v_L, w_{RK}) to (v_{LK}, w_{LK}) on the left branch of \mathcal{C}_e where $\dot{w}_e < 0$. The jumps between branches happen instantaneously with respect to the slow time scale t . Using results from [26], it is possible to show that for $\epsilon > 0$ small enough there is a periodic solution for (2.1) that is $O(\epsilon)$ (as $\epsilon \rightarrow 0$) close to the singular periodic orbit described above.

The intrinsic dynamics of I are governed by the equations

$$(2.5) \quad \begin{aligned} \epsilon v'_i &= f_i(v_i, w_i), \\ w'_i &= [w_\infty(v_i) - w_i]/\tau_i(v_i). \end{aligned}$$

Defining \mathcal{C}_i and \mathcal{S}_i analogously to the above, we choose parameters such that these two curves intersect along the left branch of \mathcal{C}_i , thus forcing the (synaptically isolated) I cell to have a global stable fixed point on the left branch of the cubic \mathcal{C}_i (Figure 3). The cell I is therefore not capable of intrinsic oscillations [29]. Fast and slow reduced equations can be defined similarly to those of E described above.

2.2. The synaptic coupling. We now describe how the synaptic coupling between cells is modeled. E has a fast excitatory synapse to I : when E is in its active state, it causes a synaptic current to be added to the right-hand side of the v'_i equation:

$$(2.6) \quad \begin{aligned} \epsilon v'_i &= f_i(v_i, w_i) - \bar{g}_{\text{exc}} H(v_e - v_{\text{thresh}})[v_i - E_{\text{exc}}], \\ w'_i &= [w_\infty(v_i) - w_i]/\tau_i(v_i), \end{aligned}$$

where H is the Heaviside function. For simplicity we have assumed that the E to I synapse is instantaneous in its effect. The Heaviside function is also used for simplicity and may be replaced by a smooth sigmoidal function in the analysis. v_{thresh} is the threshold for activation of the synapse. The parameters \bar{g}_{exc} and E_{exc} are the maximal conductance and reversal potential of the excitatory synapse, respectively. In order to simplify the bookkeeping in our analysis, we shall make the assumption that I is active if and only if E is active. This can be achieved by making E_{exc} positive

enough so that the excitatory synapse raises the cubic C_i in the phase plane, \bar{g}_{exc} large enough so that this raised cubic intersects \mathcal{S}_i along its right branch somewhere above the right knee of C_i (Figure 3), and $\tau_i(v_i)$ small enough for $v_i > v_{\text{thresh}}$. This ensures that excitation from E to I forces the I trajectory to jump to the right branch of the cubic C_i and that the I cell stays in the active state as long as E does.

The coupling from I to E is a depressing, slowly decaying inhibitory synapse. The reversal potential E_{inh} is negative enough so that inhibition lowers the cubic C_e in the phase plane. This synaptic current is described using two variables s and d ; the former models the effect of the inhibitory current on E ; the latter models the dynamics of depression. The equations which govern E become

$$\begin{aligned}
 \epsilon v'_e &= f_e(v_e, w_e) - \bar{g}_{\text{inh}}s[v_e - E_{\text{inh}}], \\
 w'_e &= [w_\infty(v_e) - w_e]/\tau_e(v_e), \\
 d' &= H(v_{\text{thresh}} - v_i)[1 - d]/\tau_\alpha - H(v_i - v_{\text{thresh}})d/\tau_\beta, \\
 \epsilon s' &= H(v_i - v_{\text{thresh}})[d - s]/\tau_\gamma - \epsilon H(v_{\text{thresh}} - v_i)s/\tau_\kappa.
 \end{aligned}
 \tag{2.7}$$

Note that d recovers towards 1 whenever I is silent and decays towards 0 whenever I is active. s decays towards 0 whenever I is silent and is reset (in the fast time scale) to the current value of d whenever I becomes active (Figure 4). Only the variable s (and not d) directly affects the behavior of E . However, since $s = d$ in the singular limit when I is active, d influences the behavior of E during the active phase. Note that, except in the transition to the active state, the inhibition to E is always decaying. On the right branch the decay is controlled by τ_β , and on the left branch the decay is controlled by τ_κ . Note also that the extent of recovery of d depends on the ratio of τ_L and τ_R (see (2.3)) and on the time constants τ_α and τ_β .

2.3. The coupled singular equations. We now define the singular equations which will be the focus of the analysis for the rest of this paper. These are equations obtained from (2.7) as above but in which we shall make a few simplifications. First, since we assume that I is active if and only if E is active, we will not explicitly track the I trajectory. We are concerned only with whether or not v_i is above or below the threshold v_{thresh} . Further, to ease the analysis, we assume that $w_\infty(v_e) = 0$ when E is in the silent state ($v_e < v_{LK}$) and $w_\infty(v_e) = 1$ when E is active ($v_e > v_{RK}$). Thus when E is in the silent state it obeys the following set of slow equations:

$$\begin{aligned}
 0 &= f_e(v_e, w_e) - s\bar{g}_{\text{inh}}[v_e - E_{\text{inh}}], \\
 w'_e &= -w_e/\tau_L, \\
 d' &= [1 - d]/\tau_\alpha, \\
 s' &= -s/\tau_\kappa.
 \end{aligned}
 \tag{2.8}$$

Alternatively, when E is in the active state it obeys the following set of slow equations:

$$\begin{aligned}
 0 &= f_e(v_e, w_e) - s\bar{g}_{\text{inh}}[v_e - E_{\text{inh}}], \\
 w'_e &= [1 - w_e]/\tau_R, \\
 d' &= -d/\tau_\beta, \\
 0 &= d - s.
 \end{aligned}
 \tag{2.9}$$

The fast equations that govern the transition from the silent to the active state are

$$\begin{aligned}
 \dot{v}_e &= f_e(v_e, w_e) - s\bar{g}_{\text{inh}}[v_e - E_{\text{inh}}], \\
 \dot{w}_e &= 0, \\
 \dot{d} &= 0, \\
 \dot{s} &= H(v_i - v_{\text{thresh}})[d - s]/\tau_\gamma,
 \end{aligned}
 \tag{2.10}$$

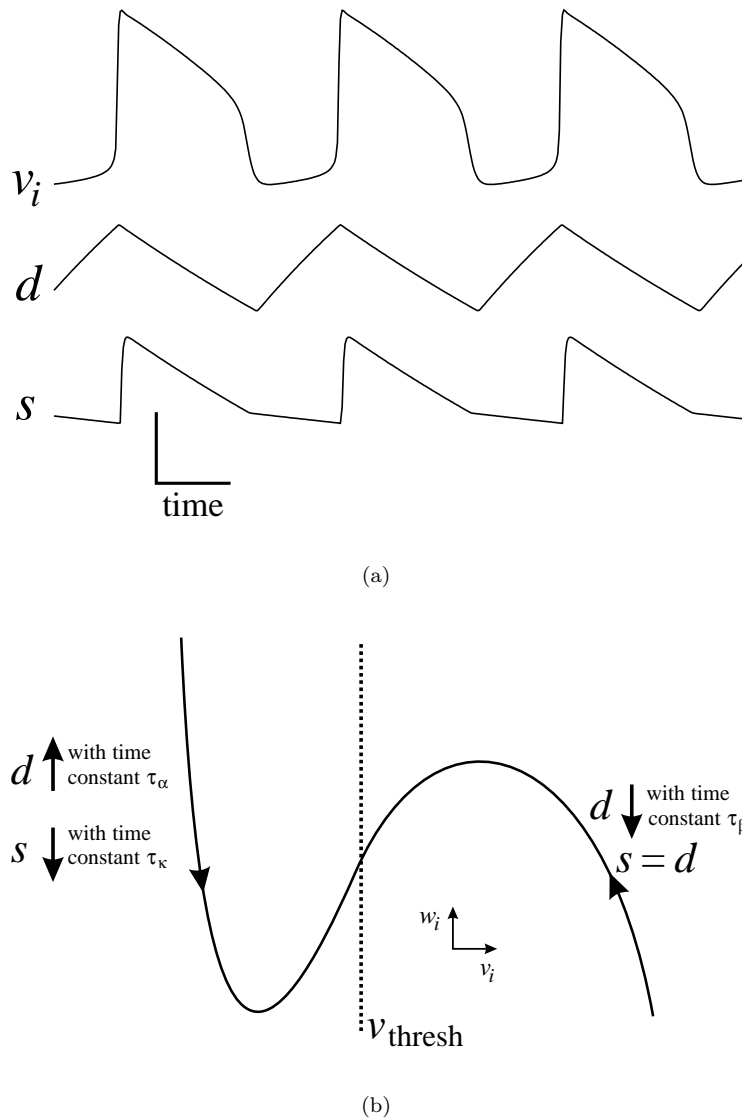


FIG. 4. Dynamics of the synaptic variables d and s . (a) Time traces of d and s depend on the oscillations of the presynaptic voltage v_i . (b) On the two branches of the v -nullcline in the I phase plane, d , and s increase or decrease with fixed time constants. v_{thresh} denotes the threshold for synaptic transmission.

and the fast equations that govern the transition from the active to the silent state are

$$(2.11) \quad \begin{aligned} \dot{v}_e &= f_e(v_e, w_e) - s\bar{g}_{\text{inh}}[v_e - E_{\text{inh}}], \\ \dot{w}_e &= 0, \\ \dot{d} &= 0, \\ \dot{s} &= H(v_i - v_{\text{thresh}})(d - s). \end{aligned}$$

The fourth equation in (2.10) shows that s is reset to d (on the fast time scale) on the transition to the active state. The fourth equation in (2.9) shows that s remains equal to d in the active phase and both decay with a time constant τ_β (Figure 4).

Our main focus will be on how the network output changes with changes of the maximal conductance \bar{g}_{inh} of the depressing synapse. We shall choose and fix the other parameters in section 3.

3. Results. We will prove the existence of two distinct oscillatory regimes for the model (2.6)–(2.7) with ϵ small and positive. The analyses of this section, however, will be performed on the reduced ($\epsilon = 0$) equations (2.8)–(2.11). Using the results of [26] on singular perturbations for the types of solutions discussed in this section, it follows that (2.6)–(2.7) have solutions that are $O(\epsilon)$ -close to their singular counterparts.

The main results of this paper are shown in Figure 5. This figure shows the bifurcation diagram of the periodic solutions of (2.6)–(2.7), where the maximum conductance \bar{g}_{inh} of the depressing synapse is varied. The solid curves correspond to stable periodic solutions. In the region of bistability, these curves are separated by an unstable periodic orbit denoted by the dashed curves. Figure 5(a) shows the minimum and maximum of v_e on the periodic orbits.

The upper branch in Figure 5(b) corresponds to stable long-period solutions, while the lower branch corresponds to stable short-period solutions. The period on the upper branch is determined by the properties of the depressing synapse, whereas on the lower branch it is largely determined by the intrinsic properties of E . We will show that for fixed $\tau_R, \tau_L, \tau_\beta$ and for τ_α and τ_κ sufficiently large there exist two maximal conductances of the depressing synapse g_* and g^* , such that if $g_* < \bar{g}_{\text{inh}} < g^*$, (2.8)–(2.11) has two stable and one unstable periodic solutions. One of the stable solutions has a period $O(\tau_L + \tau_R)$. The other has much longer period of $O(\tau_\kappa)$. Alternatively, if $\bar{g}_{\text{inh}} < g_*$, there is a unique, stable periodic solution of (2.8)–(2.11) whose period is $O(\tau_L + \tau_R)$, and if $g^* < \bar{g}_{\text{inh}}$, there is a unique stable periodic solution of (2.8)–(2.11) whose period is $O(\tau_\kappa)$.

3.1. Bistability of solutions. To construct the periodic orbits, we will define a one-dimensional Poincaré map and show that its fixed points correspond to the periodic orbits. First, we will prove that for some value of \bar{g}_{inh} the system is bistable. We will then show that for \bar{g}_{inh} small enough, or large enough, only one stable solution persists.

We stated earlier that inhibition lowers the cubic \mathcal{C}_e in the E -phase plane. For the sake of simplicity, let us assume that inhibition from I lowers only the left branch of \mathcal{C}_e (Figure 3). This assumption affects the results only minimally as we discuss below. Thus, no matter what the level of inhibition, when E is in its active state, it lies on \mathcal{C}_e and makes the transition to the silent state from (v_{RK}, w_{RK}) , the right knee of \mathcal{C}_e . Therefore, at the moment E makes the transition to the silent state, $v_e = v_{RK}$, $w_e = w_{RK}$, but the values of s and d , while equal, are unknown. This simplifying assumption enables us to define a one-dimensional Poincaré map Π at the right knee. The map Π records the value of d each time E jumps down to the silent state.

The map Π is defined by following the trajectory from the right knee back to the right knee. Start at the right knee of \mathcal{C}_e with $d(0) = d_0$. From this point, E jumps down to the silent state. Let $t = T_1$ be the time at which E jumps back up to the active state, and let $t = T_2$ be the time at which E returns to the right knee of \mathcal{C}_e . The map $\Pi : [0, 1] \rightarrow (0, 1)$ is defined by $\Pi(d_0) = d(T_2)$. If $d(T_2) = d(0) = \tilde{d}$, then \tilde{d} is a fixed point of Π , corresponding to a singular periodic solution of (2.8)–(2.11). In sections 3.2 and 3.3 we will show that for an appropriate choice of \bar{g}_{inh} , there are two values of d , $d_{\text{lo}} < d_{\text{hi}}$ such that $\Pi(d_{\text{lo}}) = d_{\text{lo}}$ and $\Pi(d_{\text{hi}}) = d_{\text{hi}}$. The fixed point d_{lo} (d_{hi}) corresponds to the periodic orbit on the lower (upper) branch of Figure 5. The time that E spends in the silent phase is the primary determinant of whether the solution

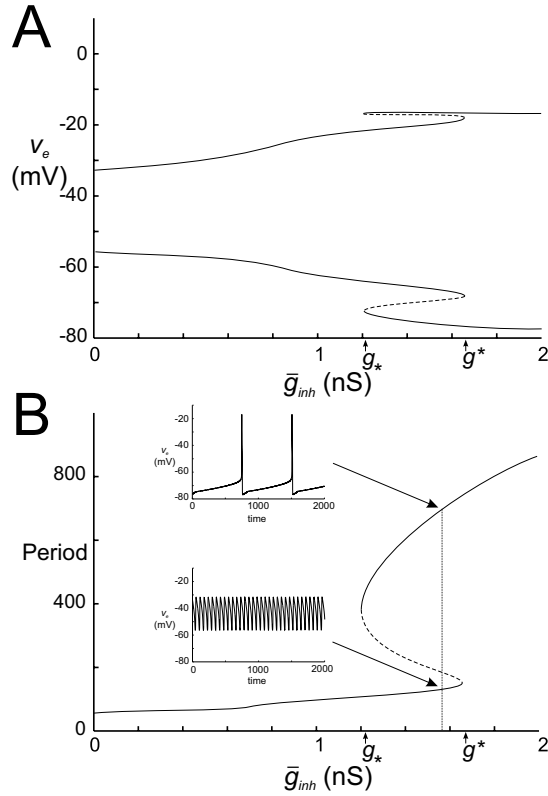
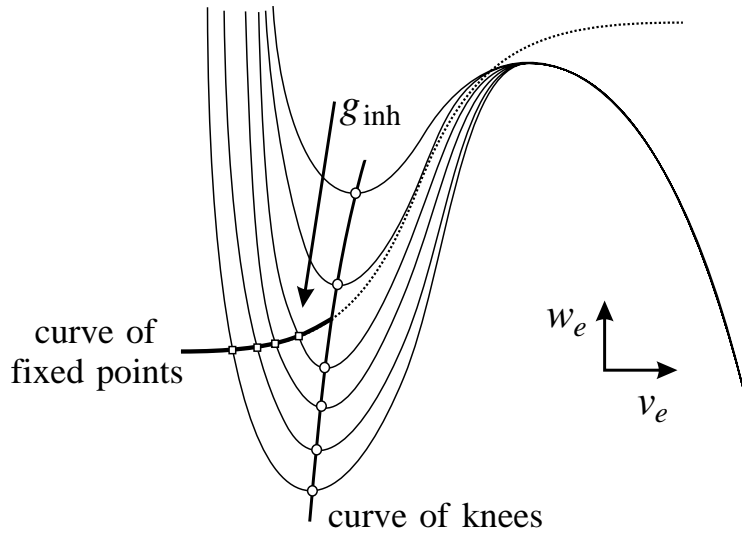


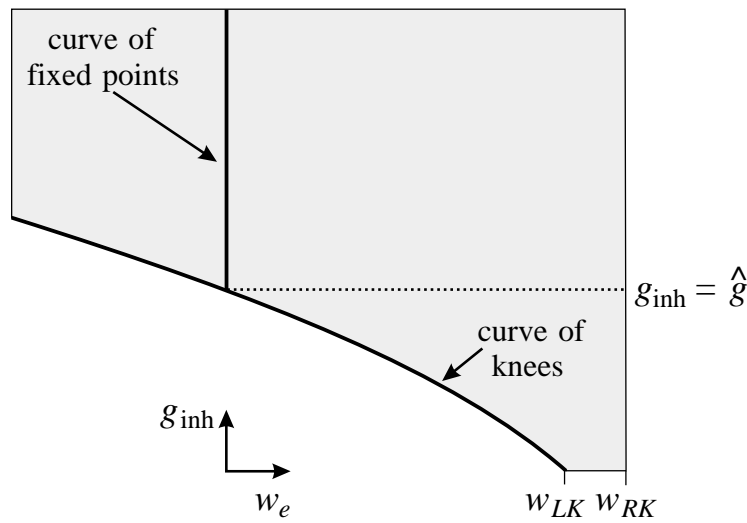
FIG. 5. Bifurcation diagram of the full system as the maximal conductance \bar{g}_{inh} of the depressing synapse is changed. Solid and dashed traces denote stable and unstable oscillations, respectively. (a) Bifurcation of the maximum and minimum values of the membrane potential of the E neuron on the periodic orbit. The inner and outer stable branches denote the cell- and synapse-dominated regimes, respectively. (b) Bifurcation diagram of the oscillation period. The lower and upper stable branches of the diagram denote the cell- and synapse-dominated regimes, respectively. Insets show the voltage traces of the E neuron for the same value of $\bar{g}_{inh} = 1.56$ nS, indicating bistability.

tends towards the higher or lower fixed points. If E spends a short time in the silent state, then d does not have enough time to recover toward 1 to compensate for its decay toward 0 in the active state. In this case, $\Pi(d)$ is attracted to d_{l0} . Alternatively, if the time spent in the silent state is relatively long, then d will recover to a value which is sufficiently large to overcome its decay in the active state. In this case, $\Pi(d)$ approaches d_{hi} .

The ratio of the time duration that E spends in its silent versus active phase is crucial in determining the evolution of d . One factor that determines the silent duration of E is the slowly decaying inhibition on the left branch of \mathcal{C}_e . Let $g_{inh} = \bar{g}_{inh}s$ and $\phi(v_e, w_e, g_{inh}) = f_e(v_e, w_e) - \bar{g}_{inh}s[v_e - E_{inh}]$. Since s is slowly decaying in the silent state (because τ_κ is large), $\phi(v_e, w_e, g_{inh}) = 0$ defines a two-dimensional slow manifold \mathcal{M} in the (w_e, g_{inh}) plane as shown in Figure 6. When E jumps down to the silent state, its trajectory on \mathcal{M} starts at $w_e = w_{RK}$ and $g_{inh} = \bar{g}_{inh}d_0$. E then



(a)



(b)

FIG. 6. Numerically generated two-dimensional slow manifold. (a) Inhibition lowers the C_e cubic in the $v - w$ phase plane. The local minima of each cubic defines a curve of knees, and the intersection of each cubic with the sigmoid defines a curve of fixed points. (b) Projection of (a) into the slow $w - g_{inh}$ phase space. The value $g_{inh} = \hat{g}$ denotes the intersection of the curve of knees $\mathcal{K}_{\mathcal{L}}$ with the curve of fixed points $\mathcal{F}_{\mathcal{L}}$ at $w = 0$. w_{LK} and w_{RK} are the w values of the left and right knees of C_e when $g_{inh} = 0$.

moves left (because $w'_e < 0$) and down (because $s' < 0$) on \mathcal{M} .

There are two important curves on \mathcal{M} : $\mathcal{K}_{\mathcal{L}}$, the set of points for which $\partial\phi/\partial v_e = 0$ and $\mathcal{F}_{\mathcal{L}}$, the set of points defined by $w'_e = 0$. $\mathcal{K}_{\mathcal{L}}$ is the curve of (left) knees representing points from which E leaves \mathcal{M} and jumps back to its active state. The second curve

$\mathcal{F}_{\mathcal{L}}$ represents a curve of stable fixed points of the reduced system (2.8) for the w_e variable. These points are not actual fixed points on \mathcal{M} because on $\mathcal{F}_{\mathcal{L}}$, $dg_{\text{inh}}/dt < 0$. For small values of g_{inh} , E is oscillatory, and hence, for these values, w_e does not have a fixed point on \mathcal{M} . Therefore, $\mathcal{F}_{\mathcal{L}}$ exists only for g_{inh} sufficiently large. Because g_{inh} is always decreasing on \mathcal{M} , E will always reach the curve of knees $\mathcal{K}_{\mathcal{L}}$ and jump back up to the active state.

Without the above assumption concerning the effect of inhibition on the right branch of \mathcal{C}_e , we would still be able to define a one-dimensional Poincaré map. However, the right branches of the E cubic would now also define a two-dimensional slow manifold, \mathcal{U} . We would need to track the position of E as it evolves along \mathcal{U} . As before, we could define a one-dimensional Poincaré map at $w_e = w_{RK}$ on \mathcal{U} . Now we would also need to measure the time it takes for the cell to evolve from $w_e = w_{RK}$ on \mathcal{U} to the curve of knees on \mathcal{U} from which it could jump down to the silent state. This time is an increasing function of d . However, for the long-period orbit, it is small compared to the time spent in the silent state, and thus the added time for which the synapse would depress would be negligible compared to the long time spent recovering. For the short-period orbit, the time is small since the time goes to zero as $d \rightarrow 0$. Thus the above assumption about the effect of inhibition on the right branch of \mathcal{C}_e does not affect the qualitative results.

3.2. The short-period orbit. Assume τ_R , τ_L , and τ_β are chosen and fixed. We will show that if τ_α is sufficiently large, there exists an interval $[0, d_*]$ which maps into itself under Π . From (3.2) it is clear that Π is continuous with respect to d . This implies the existence of a fixed point in $[0, d_*]$ which we will call d_{lo} .

Solving for d in (2.8)–(2.9), when E is silent we obtain

$$(3.1) \quad d(T_1) = 1 - (1 - d_0)e^{-T_1/\tau_\alpha},$$

and, when E is active, we obtain

$$(3.2) \quad \begin{aligned} d(T_2) &= d(T_1)e^{-(T_2-T_1)/\tau_\beta}, \\ d(T_2) &= (1 - (1 - d_0)e^{-T_1/\tau_\alpha})e^{-(T_2-T_1)/\tau_\beta}. \end{aligned}$$

Suppose $d_0 = 0$. Then it is clear that $d(T_2) > 0$, implying that $\Pi(0) > 0$. To find an appropriate d_* we need a bit more notation. Let \hat{g} be the intersection point of $\mathcal{K}_{\mathcal{L}}$ and $\mathcal{F}_{\mathcal{L}}$ (Figure 6), satisfying $\phi(v_e, 0, \hat{g}) = 0$ and $(\partial\phi/\partial v)(v_e, 0, \hat{g}) = 0$. Thus $\hat{g} = g_{\text{inh}}$ implies that $s = \hat{g}/\bar{g}_{\text{inh}}$. We choose d_* to be strictly less than $\hat{g}/\bar{g}_{\text{inh}}$, say, $d_* = \hat{g}/(2\bar{g}_{\text{inh}})$. The choice of d_* appears to be arbitrary, but later we will discuss how various parameters depend on d_* .

We need to show that $\Pi(d_*) < d_*$. The time $T_2 - T_1$ is bounded from below by T_A , the active time duration of the isolated E cell. Note that $T_A = \tau_R \log[(1 - w_{LK})/(1 - w_{RK})]$, which is $O(\tau_R)$. Therefore,

$$(3.3) \quad d(T_2) < (1 - (1 - d_*)e^{-T_1/\tau_\alpha})e^{-T_A/\tau_\beta}.$$

If the right-hand side of (3.3) is less than d_* , then so is $d(T_2)$. After rearranging terms, this condition can be written as

$$(3.4) \quad \frac{1 - d_*e^{T_A/\tau_\beta}}{1 - d_*} < e^{-T_1/\tau_\alpha}.$$

Evaluating (3.4) at $d_* = \hat{g}/(2\bar{g}_{\text{inh}})$ yields

$$(3.5) \quad \frac{2\bar{g}_{\text{inh}} - \hat{g}e^{T_A/\tau_\beta}}{2\bar{g}_{\text{inh}} - \hat{g}} < e^{-T_1/\tau_\alpha}.$$

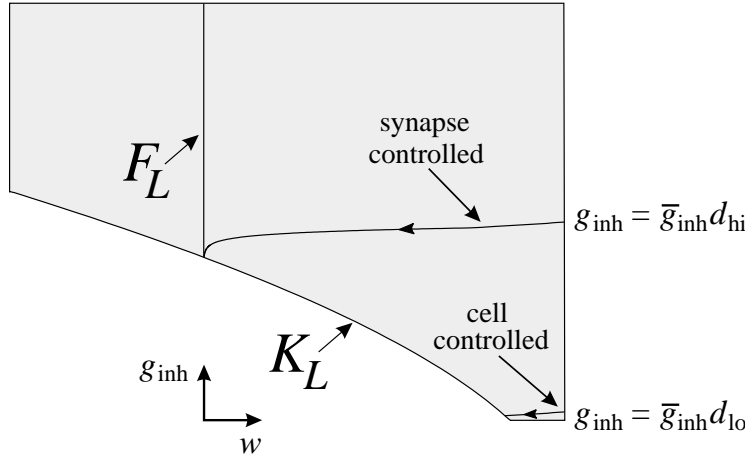


FIG. 7. Simulation results showing the trajectories of the synapse- and cell-controlled orbits projected onto the slow manifold \mathcal{M} . The cell-controlled orbit lies very close to the intrinsic E trajectory near $w = 0$. The synapse-controlled orbit lies higher on \mathcal{M} and spends a portion of its trajectory near the intersection of $\mathcal{K}_{\mathcal{L}}$ and $\mathcal{F}_{\mathcal{L}}$.

We note that the left-hand side of (3.5) is less than 1 and is independent of τ_α . In contrast, the right-hand side of (3.5) evaluated as $\tau_\alpha \rightarrow \infty$ tends to 1. Moreover, we show below that T_1 is independent of τ_α and is in fact $O(\tau_L)$. Thus if τ_α is sufficiently large, then (3.5) holds.

Suppose that the inhibition is 0 and thus, on \mathcal{M} , E travels on the curve $g_{\text{inh}} = 0$. From this curve, E jumps to the active state at $w_e = w_{LK}$ with $T_1 = T_S$, where $T_S = \tau_L \log[(1 - w_{RK})/(1 - w_{LK})]$ is the time which the isolated E cell spends in the silent state and is $O(\tau_L)$. If $d_0 = d_*$, the (s, w) trajectory of E on \mathcal{M} (see Figure 6(b)) stays above the curve $s = 0$, and thus E jumps to the active state with $w_e < w_{LK}$ and $T_1 > T_S$. Let $T_1 = T_S + T_\lambda$. The time T_λ is the time it takes E to travel from $(w_{LK}, g_{\text{inh}}(T_S))$ to the curve of knees. This time is predominantly determined by the slope of $\mathcal{K}_{\mathcal{L}}$ but is still $O(\tau_L)$. Let us assume that $\mathcal{K}_{\mathcal{L}}$ satisfies the linear relationship $\mathcal{K}_{\mathcal{L}} = \{(w_e, g_{\text{inh}}) : g_{\text{inh}} = -\lambda(w_e - w_{LK})\}$, where $-\lambda$ is the slope of $\mathcal{K}_{\mathcal{L}}$. An upper bound on T_λ is the time it takes E to go from $(w_{LK}, g_{\text{inh}}(T_S))$ to the point on $\mathcal{K}_{\mathcal{L}}$ where g_{inh} still equals $g_{\text{inh}}(T_S)$. Thus T_λ is bounded above by the time it takes w_e to evolve from w_{LK} to $w_{LK} - g_{\text{inh}}(T_S)/\lambda$. Solving (2.9), we obtain

$$(3.6) \quad T_\lambda \leq \tau_L \log \frac{\lambda w_{LK}}{\lambda w_{LK} - g_{\text{inh}}(T_S)}.$$

The argument of the log term is bounded from above independent of τ_L . Thus T_λ and therefore T_1 are also $O(\tau_L)$.

We have shown that the endpoints of the interval $[0, d_*]$ are mapped by Π into $[0, d_*]$. This implies the existence of at least one fixed point within the interval. Later we will show that this interval contains exactly one fixed point and that this point is stable. We call this fixed point d_{lo} . The period of the orbit associated with d_{lo} is $O(\tau_L + \tau_R)$ and is therefore largely determined by the intrinsic properties of E . We call this a cell-controlled orbit (Figure 7).

3.3. The long-period orbit. We now assume that τ_α is fixed at a large enough value so that d_{lo} exists, and we show that if τ_κ is sufficiently large, d_{hi} also exists.

Recall that none of the analysis of the previous section involved τ_κ ; therefore, fixing τ_κ does not affect the existence of d_{lo} .

As before, we will show that a certain interval, in this case $[d^*, 1]$, is mapped into itself by Π . Suppose first that $d_0 = 1$. Then using (3.2), $d(T_2) = e^{-T_A/\tau_\beta} < 1$. Therefore, $\Pi(1) < 1$. Assume that $d^* > \hat{g}/\bar{g}_{\text{inh}}$. As with d_* , we will later show how d^* depends on parameters. To show that $\Pi(d^*) > d^*$, we need an analogue of (3.5). As seen from the slow phase space \mathcal{M} , $w_e = 0$ is the lowest value of w from which E can jump to the active state. Therefore, $T_2 - T_1$ is bounded above by $T_{\text{max}} = \tau_R \log[1/(1 - w_{RK})]$, which is the time from $w_e = 0$ to $w_e = w_{RK}$ on the right branch of \mathcal{C}_e . A calculation similar to that of (3.3)–(3.4) shows that $\Pi(d^*) > d^*$ if

$$(3.7) \quad \frac{1 - d^* e^{T_{\text{max}}/\tau_\beta}}{1 - d^*} > e^{-T_1/\tau_\alpha}.$$

We now choose $d^* = 2\hat{g}/\bar{g}_{\text{inh}}$, where we assume that $2\hat{g} < \bar{g}_{\text{inh}}$. Evaluating (3.7) at $d^* = 2\hat{g}/\bar{g}_{\text{inh}}$, we find

$$(3.8) \quad \frac{\bar{g}_{\text{inh}} - 2\hat{g}e^{T_{\text{max}}/\tau_\beta}}{\bar{g}_{\text{inh}} - 2\hat{g}} > e^{-T_1/\tau_\alpha}.$$

Note that the left-hand side of (3.8) is again a quantity that is less than one but bounded away from zero, and is independent of T_1 . The right-hand side of (3.8) can be made arbitrarily small by making T_1 large. It is easy to make T_1 large by making τ_κ large. Suppose for the sake of argument that $\tau_\kappa \rightarrow \infty$. In this case, g_{inh} does not decay and E is attracted to $\mathcal{F}_\mathcal{L}$ and must remain in the silent state. In this case, $T_1 \rightarrow \infty$ as $\tau_\kappa \rightarrow \infty$. Clearly then, if τ_κ is sufficiently large, then T_1 will also be. For this case, (3.8) will then hold, and $\Pi(d^*) > d^*$.

As before, these two results imply that there exists $d_{\text{hi}} \in [d^*, 1]$, which is a fixed point of Π . The period of the solution associated with d_{hi} is $O(\tau_\kappa)$ and is determined by the time constant of the inhibitory decay. We call this orbit synapse-controlled (Figure 7).

3.4. Stability of orbits. We have shown that $\Pi(d^*) > d^*$ and $\Pi(d_*) < d_*$. Since Π is a continuous mapping, this implies the presence of $d_{\text{med}} \in [d_*, d^*]$ such that $\Pi(d_{\text{med}}) = d_{\text{med}}$. We now show that d_{lo} , d_{med} , and d_{hi} are the only fixed points of Π and that d_{lo} and d_{hi} are stable, while d_{med} is unstable.

A fixed point \tilde{d} of the map Π is stable if $|\Pi'(\tilde{d})| < 1$ and unstable if $|\Pi'(\tilde{d})| > 1$. This gives a local result, valid in a neighborhood of the fixed point. We will show the stronger result that $|\Pi'(d_0)| < 1$ for any $d_0 \in [0, d_*]$ or $d_0 \in [d^*, 1]$. This gives a uniform result which also implies uniqueness of the fixed points.

Using (3.2), we find that $\Pi(d_0) = d(T_1)e^{-(T_2 - T_1)/\tau_\beta}$, where T_1 and T_2 both depend on d_0 . In the following argument, let $'$ denote the derivative with respect to d_0 . A straightforward calculation using (3.1)–(3.2) and the chain rule shows that

$$(3.9) \quad \Pi'(d_0) = \left[e^{-T_1/\tau_\alpha} [1 + [1 - d_0]T_1'/\tau_\alpha] - d(T_1)[T_2 - T_1]' \right] e^{-[T_2 - T_1]/\tau_\beta}.$$

Note that $d(T_1) < 1$, τ_α is fixed, and $e^{-[T_2 - T_1]/\tau_\beta} < 1$. Therefore, by showing that $e^{-T_1/\tau_\alpha} T_1'$ and $[T_2 - T_1]'$ are small on the intervals of interest, we will have shown that the $|\Pi'| < 1$ on these intervals.

Consider first $[d^*, 1]$. If τ_κ is sufficiently large, then E jumps up from a neighborhood of $s = \hat{g}/\bar{g}_{\text{inh}}$ and $w_e = 0$. Assuming that E actually jumps up when $s = \hat{g}/\bar{g}_{\text{inh}}$

and $w_e = 0$, the time $T_2 - T_1$ is the time on the right branch that E takes to go from $w_e = 0$ to $w_e = w_{RK}$. This time is independent of d_0 , which implies that $[T_2 - T_1]' = 0$.

We next estimate $e^{-T_1/\tau_\alpha} T_1'$. For the interval $[d^*, 1]$, the time T_1 is the time it takes s to decay from d_0 to \hat{g}/\bar{g}_{inh} . Therefore, $\hat{g}/\bar{g}_{inh} = d_0 e^{-T_1/\tau_\kappa}$. Taking the derivative with respect to d_0 and using the chain rule, we find

$$0 = e^{-T_1/\tau_\kappa} - d_0 T_1' e^{-T_1/\tau_\kappa} / \tau_\kappa$$

or

$$(3.10) \quad T_1' = \tau_\kappa / d_0.$$

Thus on $[d^*, 1]$, T_1' is $O(\tau_\kappa)$. The time T_1 is bounded from above by the time it takes s to decay from 1 to \hat{g}/\bar{g}_{inh} , which is $\tau_\kappa \log(\bar{g}_{inh}/\hat{g})$. Therefore,

$$(3.11) \quad e^{-T_1/\tau_\alpha} > \left[\frac{\hat{g}}{\bar{g}_{inh}} \right]^{\tau_\kappa/\tau_\alpha}.$$

Thus e^{-T_1/τ_α} is $O(a^{\tau_\kappa})$ for some $a < 1$. This shows that $e^{-T_1/\tau_\alpha} T_1'$ is $O(\tau_\kappa a^{\tau_\kappa})$, which can be made small by making τ_κ large, independent of d_0 . As a result, if τ_κ is sufficiently large, then uniformly for all $d_0 \in [d^*, 1]$, $|\Pi'(d_0)| < 1$. This implies that d_{hi} is the unique stable fixed point on this interval.

Now consider $d_0 \in [0, d_*]$. We showed earlier that $T_1 = T_S + T_\lambda$, where T_S is the time it takes E to evolve in the silent state along $g_{inh} = 0$ and T_λ is the extra time E evolves due to the slope of the curve of knees. Clearly, $T_1' = T_\lambda'$ since T_S is independent of d_0 . There are several ways to show that T_λ' can be made small. One way is to use the slope of the curve of knees $-\lambda$. If $\lambda \rightarrow \infty$, then the curve of knees $\mathcal{K}_\mathcal{L}$ becomes vertical, and $T_\lambda \rightarrow 0$. In this case, clearly, $T_1' = T_\lambda' \rightarrow 0$ since T_1 will equal T_S which is independent of d_0 . This also implies that $[T_2 - T_1]' = 0$ in this limit as $T_2 - T_1$ will equal T_A , which is also independent of d_0 . Therefore, if we make the curve of knees more vertical, we can make $|\Pi'| < 1$.

Recall that the curve of knees is given by $\phi = 0$ and $\phi_v = 0$, where $\phi(v_e, w_e, g_{inh}) = f_e(v_e, w_e) - g_{inh}[v_e - E_{inh}]$. Let $(v_K(g_{inh}), w_K(g_{inh}))$ denote the curve of knees. Plugging this into $\phi = 0$ and differentiating with respect to g_{inh} , we find

$$0 = \phi_{v_e} \frac{\partial v_K}{\partial g_{inh}} + \phi_{w_e} \frac{\partial w_K}{\partial g_{inh}} + \phi_{g_{inh}}.$$

Using $\phi_{v_e} = 0$ and rearranging terms, we find that the slope of the curve of knees satisfies

$$(3.12) \quad \frac{\partial g_{inh}}{\partial w_K} = \frac{-\phi_{w_e}}{\phi_{g_{inh}}} = \frac{\partial f_e / \partial w_e}{v_K - E_{inh}}.$$

The slope is negative since $\partial f_e / \partial w_e < 0$ and $v_K - E_{inh} > 0$ since the synapse is inhibitory. The slope can be made large in magnitude by making $|\partial f_e / \partial w_e|$ large. This quantity is solely determined by the intrinsic properties of the cell. In our case, $|\partial f_e / \partial w_e|$ is proportional to $|g_{Ca}[v_e - E_{Ca}]|$, where g_{Ca} and E_{Ca} are the maximal conductance and reversal potential of calcium. See the appendix for the equations. The calcium reversal potential is very high, and, in particular, lies far to the right of the left branch of \mathcal{C}_e . Assuming that g_{Ca} is sufficiently large, for our equations,

$\|\partial f_e / \partial w_e\|$ is large. Therefore, we conclude that $|\Pi'| < 1$ for $d_o \in [0, d_*]$. This shows that d_{lo} is the unique stable fixed point in this interval.

The stability of the fixed points d_{lo} and d_{hi} , together with the continuity of Π , immediately implies that there exists an unstable fixed point on the interval $[d_*, d^*]$. Call this fixed point d_{med} . Note that, since it is unstable and Π is differentiable, $\Pi'(d_{med}) > 1$. To prove that it is the unique fixed point on this interval, we first note that $T_1' > 0$ on this interval. This follows since the curve of knees is negatively sloped and the evolution in the w direction is independent of d_o . The time T_1 changes from $O(\tau_L)$ to $O(\tau_\kappa)$ as d_o increases and is sigmoidal shaped. Thus T_1' has one local maximum and is relatively large at \tilde{d} . In contrast, as before $[T_2 - T_1]'$ is small. In fact, if the curve of knees is made more vertical, as above, then $[T_2 - T_1]' \rightarrow 0$. Thus using (3.9) $\Pi'(\tilde{d}) > 0$. For simplicity, assume $(T_2 - T_1)' = 0$. Then using (3.9) the magnitude of $\Pi'(d_o)$ is controlled by the term $e^{-T_1/\tau_\alpha} T_1' / \tau_\alpha$. This term has a single local maximum, which must be large since $\Pi'(d_{med}) > 1$. Since $\Pi' > 0$ and $\Pi'(d_{hi}) \leq 1$, it follows that if there is an additional fixed point between d_{med} and d_{hi} , say, \hat{d} , then $\Pi(\hat{d}) \leq 1$. But this implies that $\Pi' > 1$ on some subinterval of (\hat{d}, d_{hi}) . This, however, contradicts the fact that $e^{-T_1/\tau_\alpha} T_1' / \tau_\alpha$ has a single local maximum. Therefore, d_{med} is unique.

3.5. Existence of an interval of bistability. To complete the bifurcation diagram, we show that if \bar{g}_{inh} is too small, the system has only a single short-period orbit. Alternatively, if \bar{g}_{inh} is too large, the system has only a single large-period orbit.

Recall that \hat{g} is defined by $\phi(v_e, 0, \hat{g}) = 0$, $\phi_{v_e}(v_e, 0, \hat{g}) = 0$. Thus if $\bar{g}_{inh} < \hat{g}$, the curve of fixed points $\mathcal{F}_{\mathcal{L}}$ will not exist on the manifold \mathcal{M} . This implies that the time T_1 is largely determined by the intrinsic dynamics of the isolated E cell and there is no chance that (3.7)–(3.8) can be satisfied. Thus d_{hi} cannot exist. Moreover, if d_{hi} does not exist, d_{med} cannot exist either. Suppose to the contrary that d_{med} continues to exist. Since $\Pi(d_{med}) = d_{med}$, $\Pi'(d_{med}) > 1$, and $\Pi(1) < 1$, it must follow that there exists at least one fixed point in $(d_{med}, 1)$. This contradicts the lack of existence of d_{hi} . This finally implies that there exists a g_* such that if $\bar{g}_{inh} < g_*$, then a single small period orbit exists.

Similarly, if \bar{g}_{inh} is too large, then d_{lo} cannot exist. Suppose that $\bar{g}_{inh} \rightarrow \infty$. Then the left-hand side of (3.5) tends to 1, while the right-hand side remains less than 1. Clearly, if \bar{g}_{inh} is sufficiently large, (3.5) fails to hold. For the same reason as above, once d_{lo} disappears, d_{med} must also. Therefore, there exists a g^* such that if $\bar{g}_{inh} > g^*$, then there exists a single long-period orbit.

The analysis above provides sufficient but not necessary conditions on the time constants and conductances for the existence of an interval of bistability of solutions. In particular, the methods that we have employed show the existence of g_* and g^* but do not provide lower and upper bounds for these values.

3.6. Dependence on parameters and simulations. The existence and stability of solutions depends on the relative values of several of the time constants present in the equations. As we showed above, the short-period orbit is controlled by intrinsic parameters, while the long-period orbit is controlled by synaptic parameters. In particular, for the short-period orbit, in which the synapse remains depressed, it is important that τ_L is small relative to τ_α . Alternatively, for the long-period solution, it is important that τ_L is small relative to τ_κ . Thus the range of bistability can be expanded by varying τ_α and τ_κ . Specifically, increasing τ_α increases g^* so that the

cell-controlled range is larger. Increasing τ_κ has the effect of decreasing g_* . A slower decay of inhibition gives the synapse more time to recover in the silent state, thus allowing smaller values of the maximal conductance \bar{g}_{inh} to produce a long-period solution. By decreasing τ_α the short-period solution can be destroyed, while decreasing τ_κ destroys the long-period solution. Similar results can be obtained by fixing τ_α and varying τ_L .

In section 3, we chose d_* and d^* in a seemingly ad hoc fashion. These values also depend on the parameters in much the same way as g_* and g^* . Namely, for fixed \bar{g}_{inh} , increasing τ_α implies that d_* also increases, while increasing τ_κ decreases d^* . These changes will affect the values of the fixed points d_{hi} and d_{lo} but will not change which parameters control the existence of these fixed points.

The results shown in Figure 5 were obtained using the differential equation solver XPP together with the bifurcation continuation program AUTO. (Information on both XPP and AUTO is available at <http://www.pitt.edu/~phase>.) The maximal conductance $\bar{g}_{\text{inh}} = 1.56$ nS for both the cell- and synapse-dominated orbits. Other parameter values appear in the appendix. In Figure 8, we illustrate one way of instigating the switch mechanism with $\bar{g}_{\text{inh}} = 1.56$ nS. The oscillations start out in the cell-dominated regime in which the synapse is depressed. At $t = 525$ ms, we transiently inhibit I for 100 ms. As can be seen in the figure, the interburst interval steadily grows over the remainder of the simulation. The transient hyperpolarization initiates a regenerative loop in the dynamics whereby the additional time spent in the silent state allows the inhibitory synapse to recover more from depression. This added recovery strengthens the inhibitory synapse so that the next time E returns to the silent state more inhibition is present, and the loop repeats. The resulting orbit is synapse-controlled in which the synapse operates in the nondepressed regime. We note that the same result could be obtained by transiently hyperpolarizing E instead of I since, by our model assumptions, hyperpolarization of E effectively prohibits I from firing.

The mechanism for bistability that we described above is robust over a large set of parameter values. The analysis dictates certain relationships between the time constants but does not require specific values. To this end, the cell-dominated solutions are largely insensitive to the parameter τ_κ . The period of high-frequency oscillations was invariant to changes of at least 50% in τ_κ (simulations not shown). Alternatively, the synapse-dominated solution is insensitive to τ_L and τ_R . For τ_κ and \bar{g}_{inh} sufficiently large, the period of low-frequency oscillations is also invariant to changes of at least 50% in τ_L and τ_R .

4. Discussion. Depressing synapses are often viewed as weak or inactive synapses that are expressed only transiently when the activity rate of the presynaptic cell decreases. We showed that, in a recurrent network driven by a pacemaker cell, a transient input can initiate a regenerative process that permanently changes a depressed and insignificant synapse into a strong and influential component of the neuronal network. This process provides a switch between two mechanisms for the control of network frequency: one where the synapse is not effective and the frequency is set by the dynamics of the pacemaker and a second mechanism where the synapse is the major determinant in oscillation frequency.

We focused on a specific EI circuit where the inhibitory synapse is depressing. Because of our assumption that I is active if and only if E is active, our system is equivalent to an oscillatory I cell with a depressing inhibitory autapse. We showed that for the simple two-cell EI network, the depressing synapse is necessary for the ex-

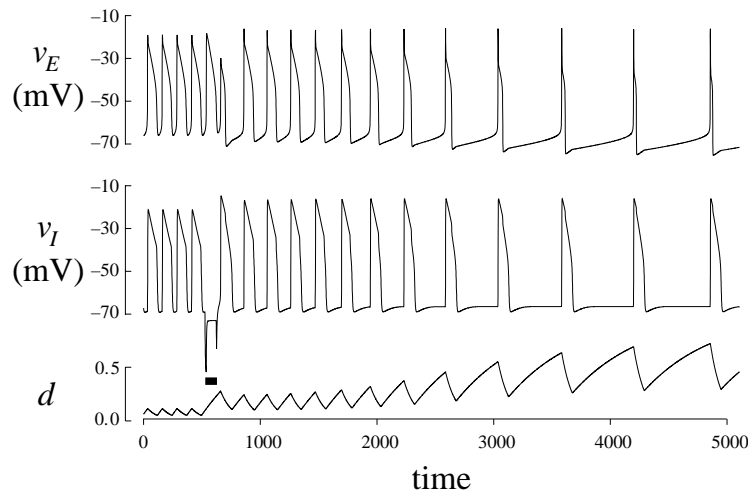


FIG. 8. *Simulation results demonstrating the bistability of solutions and a mechanism for switching between cell- and synapse-dominated orbits. The neurons begin in the cell-dominated mode, where d is small. At $t = 500$ ms we transiently hyperpolarized I for 100 ms. The lower trace shows that during the hyperpolarization d has an opportunity to grow. This resulted in a switch to the much slower synapse-dominated mode of oscillation. The black bar denotes the hyperpolarizing interval. Note that during this interval I is still excited by E .*

istence of bistability. Indeed, if synapses are nondepressing, whenever I is in its active phase, E receives the same synaptic inhibition, independent of the initial conditions or previous perturbations, and therefore remains in the same functional state.

In our analysis, we have assumed that the participating neurons make fast transitions between low (hyperpolarized) and high (depolarized) potentials. This assumption facilitated the use of geometric singular perturbation techniques that readily allowed us to dissect the model into slow and fast subsystems of lower dimension. Each of these reduced systems is controlled by a subset of the parameters of the original model. The analysis of the reduced systems, therefore, enabled us to determine which parameters control what aspects of the network output (e.g., period).

4.1. Models of synaptic depression. In the past few years, several models of synaptic depression have been proposed. Noteworthy are the models of Abbott et al. [1] and Tsodyks and Markram [34]. In both studies, the cells were modeled as integrate-and-fire neurons. Abbott et al. model synaptic depression as follows: when the presynaptic neuron produces a spike, the synaptic conductance rises instantaneously to a value $g\alpha$, and it decays to zero with a preset time constant. g is the maximal synaptic conductance, and α describes depression. The variable α recovers between presynaptic spikes and is instantaneously scaled down (depresses) by a fixed ratio whenever a spike occurs. The model of Tsodyks and Markram is based on the idea that synaptic resources are partitioned into 3 states: active, inactive, and recovered. A presynaptic spike instantaneously transfers a fixed fraction of the resources from the recovered to the active state. The active resources quickly decay to the inactive state. The inactive resources, in turn, change to recovered resources with a slower time constant.

In both models, synaptic strength is a function of interspike interval only and is totally independent of the presynaptic voltage during these intervals. However, in some neuronal systems the extent of synaptic recovery is a function of the presynaptic

voltage [22]. Moreover, the models of Abbott et al. and Markram and Tsodyks assume that the synaptic transmission terminates almost immediately after the presynaptic spike. When the sole activity of neurons is spiking, this assumption is reasonable. However, in many cases the electrical activity of neurons is more complex. For example, spiking activity may be modulated by subthreshold activity or ride on top of slow waves. In some cases, synaptic transmission can even occur in the absence of spikes but just as a result of slow variations in membrane potentials [5, 11, 22].

As in the models of Abbott et al. and Tsodyks and Markram, we view the dynamics of the synapse and the effect on the postsynaptic neuron as related but separate processes. In our model, these two processes are identical when the presynaptic cell is active but behave differently when the presynaptic cell is silent. We therefore define two variables d and s , respectively, describing the depression dynamics and the effect on the postsynaptic cell. d and s evolve with different kinetics during the silent phase: d increases (the synapse recovers), whereas s decreases (the effect on the postsynaptic cell decays). In the active phase, however, d and s are nearly identical and follow the same dynamics. Our model of synaptic depression thus lies between the model of Abbott et al., which consists of a single dynamic variable, and the model of Tsodyks and Markram, which uses two variables. Our model is, in fact, more general than these models since it takes into account factors other than the interspike interval. In particular, synaptic transmission is not dependent just on the length of the silent phase, but also on the duration of the active phase. Moreover, in our model, recovery from depression can also be dependent on the presynaptic voltage. In this work, we made the simplifying assumption that the synaptic threshold V_{thresh} is all or none. However, in the more general case, the synaptic transfer function may be smooth, and therefore the extent of d recovery could be voltage-dependent.

4.2. Bistability in neuronal systems. Both experimental and theoretical work have shown that brief perturbations (such as a short current pulse, short synaptic input, or brief exposure to a neuromodulator) can induce long-lasting changes in neuronal networks. These changes may be in the membrane potential of neurons [14], patterns of activity [8, 20], responses to input signals [15], phasing [37], coupling versus decoupling [12], firing frequency [10], or period of network oscillation [27]. Bistability in neuronal systems has been associated with a variety of functions, such as motor control [10, 18, 20], visual perception [9, 35], memory [4, 17], and representation of temporal durations [28]. In view of the wide range of behaviors attributed to neuronal bistability in its different forms, it is important to understand how bistability arises.

Bistability can be created by intrinsic neuronal properties such as voltage-gated ionic currents. For example, voltage-gated calcium currents have been associated with bistability of membrane potential in several experimental [15, 38] and theoretical [6] studies. Bistability in firing patterns can also be generated by time delays in feedback loops [19]. In rhythmic networks, bistability may be inherent to the network architecture [31, 33]. In our model, bistability of the oscillation period arises from synaptic depression. This form of bistability differs from those described in other rhythmic networks in that it involves a switch in the controlling mechanism of the periodic orbits. For example, Somers and Kopell [31] obtain bistability between synchronous and antiphase solutions in mutually coupled excitatory networks. However, in their model the periods of both solutions are completely determined by the intrinsic properties of the cells. In our model, the bistability of periodic orbits does not merely imply that the network can be switched from one periodic solution to the other by a transient input. The interesting and perhaps more profound result of the switch is

that a component of the network that was previously ineffective is now in control of the network frequency. This may have important implications for neuromodulation, as discussed below.

4.3. The role of network parameters. The cell-dominated regime, or short-period orbit, is controlled by the intrinsic neuronal properties, such as the time constants τ_L and τ_R that govern the time intervals spent on the left and right branches in the absence of synaptic input. This mode of oscillation persists as long as the depressing synapse is prevented from recovering. For example, if the time constant of synaptic recovery τ_α is much larger than τ_L (or the time constant of depression τ_β is much smaller than τ_R), the oscillation will be cell-dominated, unless the maximal synaptic conductance \bar{g}_{inh} is unrealistically large. Because the depressing synapse is weak in this regime, the oscillation period is mostly insensitive to changes in the synaptic time constants τ_κ , τ_α , or τ_β . However, sufficient decrease of τ_α relative to τ_L (or increase of τ_β relative to τ_R) will switch the system to the synapse-dominated regime, where these synaptic parameters are the most important factors in determining the oscillation period. In the synapse-dominated regime, τ_L and τ_R do not affect the oscillation period.

The range of the bistable regime is determined by the synaptic time constants τ_κ , τ_β , and τ_α . An increase in τ_α will weaken the synapse by slowing down recovery from depression and hence push g^* (the turning point of the cell-dominated branch) to the right. A similar effect is obtained by decreasing τ_β and hence speeding up depression. Alternatively, increasing τ_κ enables the synapse to remain effective for a longer time when the cells are in their inactive state. Thus increasing τ_κ will push g_* (the turning point of the synapse-dominated branch) to the left. Decreasing τ_κ or τ_α (or increasing τ_β) sufficiently could cause the two turning points g_* and g^* to coalesce, thereby destroying the bistable regime.

The mechanism for bistability that we described applies quite generally to a variety of network architectures. For example, if the excitatory synapse is the one that shows depression, or if both synapses are depressing, the two modes of oscillation may still be present and overlap to produce bistability. In fact, a network with two depressing synapses with distinct time scales may have a separate switch mechanism for each synapse, potentially providing multiple oscillatory regimes (dominated by the intrinsic properties of the cells, by one synapse, or by both synapses).

4.4. Significance for modulation of rhythmic networks. The rhythmic network that we have analyzed has the capability to regulate its frequency upon arrival of the appropriate signal. Long-lasting changes in oscillation period can be triggered by an appropriately timed, brief synaptic, or modulatory input. For instance, if the system is operating in the cell-dominated regime, an inhibitory input that occurs during and prolongs the silent phase can have a large impact on the system because it will allow recovery from depression and switch the system to the synapse-dominated regime. However, the same input during the active phase of the cell-dominated oscillation will be mostly ignored because the depressed synapse cannot recover during this phase. In this case, the perturbation will merely generate a time shift of the oscillation.

Our work also demonstrates that some parameters affect the oscillation period orbit only in the synapse-dominated regime and not in the cell-dominated regime. For example, in the cell-dominated regime the network is largely insensitive to changes in the decay time constant of synaptic inhibition. In contrast, in the synapse-dominated regime this parameter is important and determines the duration of the interburst

phase. This allows the neuronal circuit to be primed (for example, by a modulatory effect that prolongs the decay time constant) for the change in control, without any apparent change in output, prior to the occurrence of a triggering event. Hence a neuronal circuit in the cell-dominated regime would switch to the synapse-dominated regime in two steps. A similar mechanism has been described in the endogenous burster R15 in *Aplysia*, where electrical activity changes from bursting to beating following a brief perturbation but only in the presence of serotonin [20]. This procedure could be used as a safety mechanism to prevent the system from accidentally switching from one activity mode to another, for example, as a result of synaptic noise.

Neural networks are largely controlled by neuromodulation. Often, neuromodulation is used for fine tuning of functional circuits [23]. However, in many cases neuromodulation can produce far more extensive changes. For instance, neuromodulation can switch neurons to participate at different times in distinct functional circuits [13, 25]. Also, neuromodulation can reconfigure neuronal circuits [24] so that the same hardware can be used to produce different outputs, thereby adding to the flexibility of neural networks. Despite the wide impact of neuromodulation on neural activity, many aspects of neuromodulatory action are not well understood. For example, in most cases it is not known whether modulators affect neural networks by targeting cellular and/or synaptic components directly or whether they modify the networks by changing one component of the network, thereby triggering a cascade of events that leads to a new network output. We propose that in a neuronal network that includes depressing synapses, modulatory effects that change the dynamics of these synapses are sufficient to reconfigure the entire network. Such a mechanism could allow the network to utilize components that were previously functionally insignificant or to remove components that were previously important.

Appendix. The equations that we used for the simulations in Figures 5–8 are as follows:

$$(A.1) \quad C v' = I_{\text{ext}} - I_{C_a} - I_{\text{leak}} - I_{\text{syn}},$$

$$(A.2) \quad w' = [w_{\infty}(v) - w]/\tau(v),$$

where $I_{C_a} = g_{C_a} m_{\infty}(v)[1-w][v-E_{C_a}]$, $I_{\text{leak}} = g_{\text{leak}}[v-E_{\text{leak}}]$, and I_{ext} is an external tonic current. All voltages are in mV , time constants are in msec, and conductances are in nS . The functions m_{∞} and w_{∞} have the form $1/(1 + \exp(-(v - x_1)/x_2))$. The function $\tau = \tau_L + [\tau_R - \tau_L]h_{\infty}(v)$. Common parameter values for both cells are $E_{C_a} = 0$, $E_{\text{leak}} = -65$, $g_{C_a} = 1.6$, $g_{\text{leak}} = 0.3$, $C = 1$, $\tau_L = 50$, $\tau_R = 50$, and, for m_{∞} , $x_1 = -50$, $x_2 = 4$. For the E cell we used $I_{\text{ext}} = 0$ and for w_{∞} , $x_1 = -53$ and $x_2 = 1$; for the I cell we used $I_{\text{ext}} = -1.5$ and $x_1 = -64$ and $x_2 = 6$.

The excitatory synaptic current from E to I is given by $\bar{g}_{\text{exc}} s_e(v_i - E_{\text{exc}})$, where $g_e = 0.1$ and $E_{\text{exc}} = 0$. The variable $s_e = 1/(1 + \exp(-(v_e - x_1)/x_2))$ with $x_1 = -53$ and $x_2 = 1$. The inhibitory current from I to E is of the form $\bar{g}_{\text{inh}} s_i(v_e - E_{\text{inh}})$ with $E_{\text{inh}} = -80$. The synaptic variable s_i and the depression variable d_i obey

$$(A.3) \quad s'_i = [d_i s_{\infty}(v_i) - s_i]/\tau_{s_i}(v_i),$$

$$(A.4) \quad d'_i = [d_{\infty}(v_i) - d_i]/\tau_{d_i}(v_i),$$

where $s_{\infty}(v_i) = 1/(1 + \exp(-(v_i - v_{\text{thresh}})/x_2))$ with $v_{\text{thresh}} = -64$ and $x_2 = 6$, $\tau_{s_i}(v_i) = \tau_{\kappa} + [\tau_{\gamma} - \tau_{\kappa}]s_{\infty}(v_i)$ with $\tau_{\gamma} = 1$, $\tau_{\kappa} = 500$, $d_{\infty}(v_i) = 1/[1 + \exp(v_i - v_{\text{rec}})]$ with $v_{\text{rec}} = -55$, and $\tau_{d_i}(v_i) = \tau_{\beta} + [\tau_{\alpha} - \tau_{\beta}]d_{\infty}(v_i)$ with $\tau_{\alpha} = 600$ and $\tau_{\beta} = 100$.

REFERENCES

- [1] L. F. ABBOTT, J. A. VARELA, K. SEN, AND S. B. NELSON, *Synaptic depression and cortical gain control*, *Science*, 275 (1997), pp. 220–224.
- [2] Y. ADINI, D. SAGI, AND M. TSODYKS, *Excitatory-inhibitory network in the visual cortex: Psychophysical evidence*, *Proc. Natl. Acad. Sci. USA*, 94 (1997), pp. 10426–10431.
- [3] D. G. AMARAL AND M. P. WITTER, *Hippocampal formation*, in *The Rat Nervous System*, G. Paxinos, ed., Academic Press, San Diego, pp. 443–493.
- [4] C. A. BARNES, M. S. SUSTER, J. SHEN, AND B. L. MCNAUGHTON, *Multistability of cognitive maps in the hippocampus of old rats*, *Nature*, 388 (1997), pp. 272–275.
- [5] M. BURROWS AND M. V. S. SIEGLER, *Graded synaptic transmission between local interneurons and motoneurons in the metathoracic ganglion of the locust*, *J. Physiol. (Lond.)*, 285 (1978), pp. 231–255.
- [6] V. BOOTH AND J. RINZEL, *A minimal, compartmental model for a dendritic origin of bistability of motoneuron firing patterns*, *J. Comput. Neurosci.*, 2 (1995), pp. 299–312.
- [7] D. BUONOMANO, *Decoding temporal information: A model based on short-term synaptic plasticity*, *J. Neurosci.*, 20 (2000), pp. 1129–1141.
- [8] K. P. CARLIN, K. E. JONES, Z. JIANG, L. M. JORDAN, AND R. M. BROWNSTONE, *Dendritic L-type calcium currents in mouse spinal motoneurons: Implications for bistability*, *European J. Neurosci.*, 12 (2000), pp. 1635–1646.
- [9] K. E. EASTMAN AND H. S. HOCK, *Bistability in the perception of motion and stationarity: Effects of temporal asymmetry*, *Percept. Psychophys.*, 61 (1999), pp. 1055–1065.
- [10] T. EKEN, H. HULTBORN, AND O. KIEHN, *Possible functions of transmitter-controlled plateau potentials in alpha motoneurons*, *Prog. Brain Res.*, 80 (1989), pp. 257–267.
- [11] K. GRAUBARD, *Synaptic transmission without action potentials: Input-output properties of a nonspiking presynaptic neuron*, *J. Neurophysiol.*, 41 (1978), pp. 1014–1025.
- [12] A. L. HARRIS, D. C. SPRAY, AND M. V. BENNETT, *Control of intercellular communication by voltage dependence of gap junctional conductance*, *J. Neurosci.*, 3 (1983), pp. 79–100.
- [13] S. L. HOOPER AND M. MOULINS, *Switching of a neuron from one network to another by sensory-induced changes in membrane properties*, *Science*, 244 (1989), pp. 1587–1589.
- [14] J. HOUNSGAARD, H. HULTBORN, B. JESPERSEN, AND O. KIEHN, *Bistability of alpha-motoneurons in the decerebrate cat and in the acute spinal cat after intravenous 5-hydroxytryptophan*, *J. Physiol. (Lond.)*, 405, (1988), pp. 345–67.
- [15] S. W. HUGHES, D. W. COPE, T. I. TOTH, S. R. WILLIAMS, AND V. CRUNELLI, *All thalamocortical neurons possess a T-type Ca^{2+} “window” current that enables the expression of bistability-mediates activities*, *J. Physiol. (Lond.)*, 517 (1999), pp. 805–815.
- [16] E. G. JONES, *Connectivity of the primate sensory-motor cortex*, in *Cerebral Cortex*, Vol. 5, E. G. Jones and A. Peter, eds., Plenum Press, New York, 1986, pp. 113–183.
- [17] A. B. KIRILLOV, C. D. MYRE, AND D. J. WOODWARD, *Bistability, switches and working memory in a two-neuron inhibitory-feedback model*, *Biol. Cybernet.*, 68 (1993), pp. 441–449.
- [18] D. KLEINFELD, F. RACCUA-BEHLING, AND H. J. CHIEL, *Circuits constructed from identified Aplysia neurons exhibit multiple patterns of persistent activity*, *Biophys. J.*, 57 (1990), pp. 697–715.
- [19] S. KUNEC AND A. BOSE, *Role of axonal delays in organizing the behavior of self-inhibiting neurons*, *Phys. Rev. E*, 63 (2001), 0219081-13.
- [20] H. A. LECHNER, D. A. BAXTER, J. W. CLARK, AND J. H. BYRNE, *Bistability and its regulation by serotonin in the endogenously bursting neuron R15 in Aplysia*, *J. Neurophysiol.*, 75 (1996), pp. 957–962.
- [21] J. LISMAN, *Bursts as a unit of neuronal information: Making unreliable synapses reliable*, *Trends Neurosci.*, 20 (1997), pp. 38–43.
- [22] Y. MANOR, F. NADIM, L. F. ABBOTT, AND E. MARDER, *Temporal dynamics of graded synaptic transmission in the lobster stomatogastric ganglion*, *J. Neurosci.*, 17 (1997), pp. 5610–5621.
- [23] E. MARDER AND J. M. WEIMANN, *Modulatory control of multiple task processing in the stomatogastric nervous system*, in *Neurobiology of Motor Program Selection*, J. Kien, C. McCrohan, and B. Winlow, eds., Pergamon Press, New York, 1992, pp. 3–19.
- [24] E. MARDER, J. C. JORGE-RIVERA, V. KILMAN, AND J. M. WEIMANN, *Peptidergic modulation of synaptic transmission in a rhythmic motor system*, in *The Synapse: In Development, Health, and Disease*, B. W. Festoff, D. Hanta, and B. A. Ctron, eds., JAI Press, Greenwich, CT, 1997, pp. 213–233.
- [25] P. MEYRAND, J. SIMMERS, AND M. MOULINS, *Construction of a pattern-generating circuit with neurons of different networks*, *Nature*, 351 (1991), pp. 60–63.

- [26] E. F. MISHCHENKO, Y. S. KOSELEV, A. Y. KOSELEV, AND N. K. ROZOV, *Asymptotic Methods in Singularly Perturbed Systems*, Monogr. Contemp. Math., Revaz Gamkrelidze, ed., Consultants Bureau, New York, London, 1994.
- [27] F. NADIM, Y. MANOR, N. KOPELL, AND E. MARDER, *Synaptic depression creates a switch that controls the frequency of an oscillatory circuit*, Proc. Natl. Acad. Sci. USA, 96 (1999), pp. 8206–8211.
- [28] H. OKAMOTO AND T. FUKAI, *A model for neural representation of temporal duration*, Biosystems, 55 (2000), pp. 59–64.
- [29] J. RINZEL AND G. B. ERMENTROUT, *Analysis of neural excitability and oscillations*, in Methods in Neuronal Modeling: From Ions to Networks, C. Koch and I. Segev, eds., MIT Press, Cambridge, MA, 1998, pp. 251–291.
- [30] M. E. SCHEIBEL AND A. B. SCHEIBEL, *Structural organization of nonspecific thalamic nuclei and their projection toward cortex*, Brain Res., 6 (1967), pp. 60–94.
- [31] D. SOMERS AND N. KOPELL, *Rapid synchronization through fast threshold modulation*, Biol. Cybernet., 68 (1993), pp. 393–407.
- [32] J. W. S. TABAK, M. O'DONNOVAN, AND J. RINZEL, *Modeling of spontaneous activity in developing spinal cord using activity-dependent depression in an excitatory network*, J. Neurosci., 20 (2000), pp. 3041–3056.
- [33] D. TERMAN, N. KOPELL, AND A. BOSE, *Dynamics of two mutually coupled slow inhibitory neurons*, Phys. D, 117 (1998), pp. 241–275.
- [34] M. V. TSODYKS AND H. MARKRAM, *The neural code between neocortical pyramidal neurons depends on neurotransmitter release probability*, Proc. Natl. Acad. Sci. USA, 94 (1997), pp. 719–723.
- [35] G. VETTER, J. D. HAYNES, AND S. PFAFF, *Evidence for multistability in the visual perception of pigeons*, Vision Res., 40 (2000), pp. 2177–2186.
- [36] J. VOOGD AND M. GLICKSTEIN, *The anatomy of the cerebellum*, Trends Neurosci., 21 (1998), pp. 370–375.
- [37] J. L. WILKENS AND R. E. YOUNG, *Patterns and bilateral coordination of scaphognathite rhythms in the lobster *Homarus americanus**, J. Exp. Biol., 63 (1975), pp. 219–235.
- [38] S. R. WILLIAMS, T. I. TOTH, J. P. TURNER, S. W. HUGHES, AND V. CRUNELLI, *The “window” component of the low threshold Ca^{2+} current produces input signal amplification and bistability in cat and rat thalamocortical neurons*, J. Physiol. (Lond.), 505 (1997), pp. 689–705.
- [39] E. ZUCKER, *Calcium- and activity-dependent synaptic plasticity*, Curr. Opin. Neurobiol., 9 (1999), pp. 305–313.